Neutron Transfer and the Tunneling Mechanism in the Bombardment of Gold by Nitrogen*

J. A. McIntyre, T. L. Watts, and F. C. Jobes
Yale University, New Haven, Connecticut
(Received March 17, 1960)

Measurements have been made of the angular distributions of N^{13} nuclei produced in the neutron-transfer reaction $Au^{197}(N^{14},N^{13})Au^{198}$. Fifteen different bombarding energies were studied. It is found that the results can be described in terms of the transfer of a neutron from an N^{14} nucleus moving along a classical trajectory. In particular, it is found that N^{14} trajectories with distances of closest approach of $(12.7\pm0.5)\times10^{-13}$ cm give the largest contribution to the transfer process. Further, both the angular and energy dependence of the N^{13} production have been compared with the dependences predicted by the tunneling theory of Breit and Ebel; both experimental dependences have been found to be in agreement with this theory.

I. INTRODUCTION AND SUMMARY

A NUMBER of years ago, Breit, Hull, and Gluckstern[1] pointed out that conditions at the nuclear surface could be investigated by the study of the transfer of a nucleon from a bombarding nucleus to a target nucleus. The well-known deuteron stripping mechanism is an example, of course, of such a nucleon transfer. However, as was emphasized by Breit, Hull, and Gluckstern, a great computational advantage is gained by studying the transfer from nuclei much heavier than the mass of the transferred nucleon. If this condition of a massive bombarding nucleus is obtained, the motion of the bombarding nucleus can be considered classically and only the nucleon transfer itself need be considered quantum mechanically. The quantum-mechanical transfer mechanism would be expected to be relatively simple, being describable in terms of the tunneling of a nucleon from the potential well of the bombarding nucleus to the potential well of the target nucleus. Experimental measurements of this process would then yield information about the wave function of the transferred nucleon in its bound state in both of the interacting nuclei.

Since this initial discussion of the nucleon-transfer problem, there has been considerable activity, both experimental and theoretical, concerned with the investigation of the mechanism of the transfer of nucleons. A critique of this work has been published by Breit[2] who has evaluated the status of the problem as of recent date. The facts relevant to the present paper are the following.

The first experiments performed to study the transfer reaction in detail were those of Reynolds and Zucker,[3] the reaction under investigation being the $N^{14}(N^{14},N^{13})N^{15}$ reaction. Total cross sections for the reaction were measured as a function of energy while angular distributions of the N^{13} nuclei were determined at several energies. A careful analysis of the neutron transfer tunneling mechanism was then made by Breit and Ebel[4] who also compared the experimental data with the predictions of the tunneling theory. It was found that neither the experimental dependence of the total cross section on energy, nor the angular distribution results agreed with the tunneling theory. However, by including the possibility of virtual-state formation due to the Coulomb interaction between the colliding nuclei Breit and Ebel,[5] in another paper, were able to obtain agreement between the experimental data and the nucleon transfer theory. Unfortunately, the transfer process was now much more complicated and it became doubtful whether information about nuclear wave functions could be obtained. However, further experimental information in the form of angular distributions from the $Mg^{25}(N^{14},N^{13})Mg^{26}$ transfer reaction was obtained by Halbert and Zucker.[6] It was shown by Breit[2] that these data were approximately represented by the tunneling theory and were at least partially consistent with it. Other angular distribution data by Volkov, Pasiuk, and Flerov,[7] and by Hubbard and Merkel[8] as well as a number of excitation functions measured at Oak Ridge[9] have not yet been compared with theory. Present knowledge concerning the neutron transfer mechanism is therefore incomplete. The following experimental work on the neutron transfer reaction, $Au^{197}(N^{14},N^{13})Au^{198}$, is presented so that additional information may be available for the study of this problem.

The experimental results to be presented consist of 25 angular distributions taken at 15 different energies. The energy resolution of the experiment (2.3 Mev) was not sufficiently good to separate interactions exciting the various levels of the residual Au^{198} nucleus; never-

* This work was supported by the U. S. Atomic Energy Commission.

[1] G. Breit, M. H. Hull, and R. L. Gluckstern, Phys. Rev. **87**, 74 (1952).

[2] G. Breit, *Handbuch der Physik*, edited by S. Flügge (Springer-Verlag, Berlin, 1959), Vol. **XLI**, Part 1, pp. 367–407.

[3] H. L. Reynolds and A. Zucker, Phys. Rev. **101**, 166 (1956).

[4] G. Breit and M. E. Ebel, Phys. Rev. **103**, 679 (1956).

[5] G. Breit and M. E. Ebel, Phys. Rev. **104**, 1030 (1956).

[6] M. L. Halbert and A. Zucker, Phys. Rev. **108**, 336 (1957).

[7] V. V. Volkov, A. S. Pasiuk, and G. N. Flerov, J. Exptl. Theoret. Phys. (U.S.S.R.) **33**, 595–601 (1957) [translation: Soviet Phys.—JETP **6**, 459 (1958)].

[8] E. L. Hubbard and G. Merkel, Proceedings of the Conference on Reactions between Complex Nuclei [Oak Ridge National Laboratory Report ORNL-2606, 1958 (unpublished)].

[9] D. E. Fisher, A. Zucker, and A. Gropp, Phys. Rev. **113**, 542 (1959).

theless it was good enough to show that in the transfer process the Au^{198} nucleus can become highly excited and, in fact, the neutron may even be captured in a continuum state. The evidence for this is shown in Fig.2 where a range measurement has been made of the N^{13} nuclei leaving the Au^{197} target. The N^{13} nuclei are indicated by the ● symbol and are seen to have a long range with a spread in range corresponding to an energy spread of ~7 Mev. The 2.3-Mev resolution is seen to be much narrower than this spread in N^{13} energy. The width of the N^{13} peak must therefore be due to excitation of the Au^{198} nuclei. In the measurements of the angular distributions to be reported here, all of the N^{13} nuclei in the peak in Fig. 2 were detected.

The angular distributions obtained for the N^{13} nuclei are shown in Fig. 6. All differential cross sections, angles, and energies are for the center-of-mass system. The letters indicate experimentally-measured cross section values, a different letter being assigned to each N^{14} bombarding energy. A smooth curve has been drawn through each set of letters; thus, all data shown in Fig. 6 are experimental. It is seen that the cross sections peak at some angle for each bombarding energy and that the peaks move to larger angles with decreasing energy. Such a behavior would be expected for particles following classical Rutherford scattering trajectories if there were some interaction radius, R_a, such that (1) outside R_a, the transfer probability drops off with increasing radius, and (2) inside R_a, the N^{14} nuclei are absorbed. It is therefore convenient to describe the scattering in terms of a radius instead of in terms of a scattering angle. The radius associated with a particle trajectory is $R_{\min}$, the distance of closest approach to the scattering center; it is related to the scattering angle θ for Rutherford scattering by the equation

$$R_{\min}=(ZZ'e^2/2E)[1+\csc(\theta/2)],$$

where Ze and $Z'e$ are the charge of the N^{14} and Au^{197} nuclei, and E is the energy of the system. The differential cross sections, $d\sigma/dR_{\min}$, have been computed from the experimental values for $d\sigma/d\Omega$ plotted in Fig. 6 [see Eq. (4) in Sec. IV for this transformation]. The $d\sigma/dR_{\min}$ values have then been plotted against $R_{\min}$ in Fig. 7 on a logarithmic scale. In this figure, the data for each energy have been normalized to unity at the peak of the curve. Again, the letters represent experimentally-measured cross sections.

Inspection of Fig. 7 reveals clearly that the neutron transfer process takes place chiefly from a set of trajectories having distances of closest approach near a fixed value. (The nitrogen trajectories are assumed to be undisturbed by the transfer of the neutron.) This critical distance of closest approach is the same for all of the energies studied and hence for trajectories with large or small deflections and for N^{14} nuclei with high or low velocities as they pass the Au^{197} nuclei. The value for $R_{\min}$ at the peak of the experimental points in Fig. 7 is a measure of R_a, the radius at which absorption of the N^{14} nuclei begins. The value of $R_{\min}$ (peak) $\sim R_a$ is found from Fig. 7 to be $(12.7\pm0.5)\times10^{-13}$ cm. This value corresponds to an r_0 of $(1.55\pm0.06)\times10^{-13}$ cm, where r_0 is defined by the equation $R_{\min}=r_0(A_1^{\frac{1}{3}}+A_2^{\frac{1}{3}})$, A_1 and A_2 being the atomic weights of the N^{14} and Au^{197} nuclei. The fact that the many curves in Fig. 6 can be merged by a classical transformation into the normalized peak in Fig. 7 is impressive evidence for the validity of the argument of Breit, Hull, and Gluckstern[1] that heavy particle interactions can be studied partially by classical means.

From the form of the curve defined by the experimental points in Fig. 7, a qualitative description of the transfer mechanism can be given. For large $R_{\min}$ (N^{14} trajectories which do not approach closely to the Au^{197} nucleus) there is little neutron transfer. The transfer builds up rapidly, however, as $R_{\min}$ decreases. This effect shows the strong radial dependence of the transfer mechanism. On the other hand, for small values of $R_{\min}$, the transfer process is again unlikely. This can be explained in terms of the strong absorption by the Au^{197} nucleus of N^{14} nuclei on trajectories passing inside an absorption radius, R_a. From the elastic scattering of C^{12} on Au^{197} it has been shown[10] that the absorption radius between Au^{197} and C^{12} has an r_0 of 1.47×10^{-13} cm, which is approximately the same as the r_0 value revealed by the neutron transfer data just presented. Thus, as $R_{\min}$ is decreased from large values, the transfer process increases until the absorption radius is reached; as $R_{\min}$ continues to decrease, the attenuation of the N^{14}-N^{13} nuclei by absorption in the Au^{197} nucleus reduces the transfer cross section again.

The data in Fig. 7 can also be compared with the tunneling theory of Breit and Ebel.[4] This theory would be expected to apply only for large values of $R_{\min}$ where there is no absorption by the Au^{197} nucleus. The dependence of neutron transfer on $R_{\min}$ according to the tunneling theory has been indicated in Fig. 7 by the solid curve which has been normalized to the experimental data. It is seen that the tunneling theory gives a reasonably good description of the transfer reaction, at least at the lower bombarding energies (the later letters in the alphabet in Fig. 7).

A further test of the tunneling theory can be made by studying the total cross sections for the reaction. From the data in Fig. 6, as well as similar data not shown there, total cross sections are obtained for the various energies by integrating over all angles. The total cross sections, σ, so obtained are plotted in Fig. 8 against energy. The steep rise for σ at low energies corresponds to the increase in the transfer mechanism as the N^{14} trajectories approach closer to the Au^{197} nucleus; the levelling off occurs when trajectories penetrate inside the absorption radius, R_a. The prediction of the tunneling theory[4] is shown by the solid line and

[10] E. Goldberg and H. L. Reynolds, Phys. Rev. **112**, 1981 (1958).

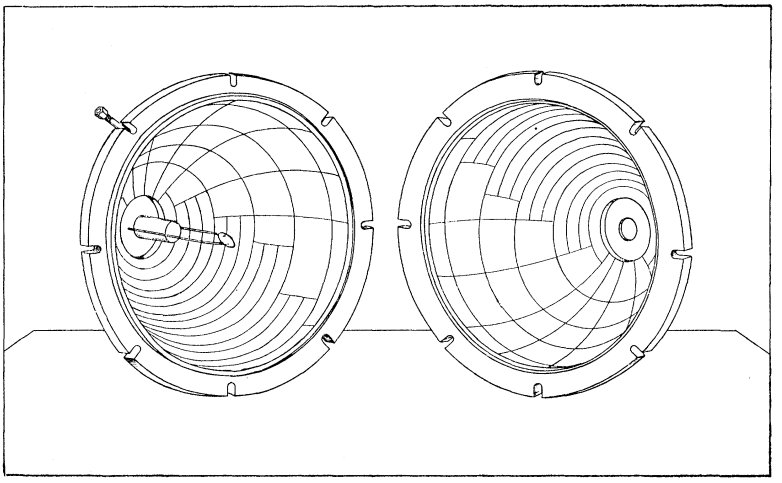

FIG. 1. Isometric view of the spherical reaction chamber shown in its dismantled condition.

is normalized to the data. It is seen to fit the experimental points over the region where absorption does not occur.

The two tests of the tunneling theory just made are independent as may be seen by referring to the primary data which have been shown in Fig. 6. The areas under the peaks in Fig. 6 are closely related to the total cross sections plotted in Fig. 8. On the other hand the shapes of the curves in Fig. 6 have been displayed in a common plot by means of Fig. 7. Since the tunneling theory has been seen to be consistent with the data in both Figs. 7 and 8, it is consistent with both the areas under the peaks in Fig. 6 and the shapes of the peaks in Fig. 6. Thus, by two independent comparisons, the tunneling theory is seen to be consistent with the experimental data.

In conclusion then, these experiments (1) show the validity of studying the neutron transfer process by semiclassical means, (2) yield an absorption radius for the interaction of N^{14} and Au^{197} nuclei of $(12.7+0.3)\times10^{-13}$ cm, and (3) within the limitations of the present somewhat preliminary considerations are consistent with the tunneling theory of Breit and Ebel[4] as shown by two independent comparisons between experiment and theory.

II. EXPERIMENTAL APPARATUS

A. General Description

Experimentally, the study of the $Au^{197}(N^{14},N^{13})Au^{198}$ reaction is similar to a scattering experiment. The detector for the N^{13} nuclei is placed at various angles, θ, with respect to the beam direction. The number of N^{13} nuclei produced are then counted as a function of angle, θ, and bombarding energy E.

The basic experimental problem is to distinguish the desired N^{13} nuclei from N^{14} nuclei which have been elastically scattered from the Au^{197} target nuclei. The elastic scattering differential cross section is approximately the Rutherford scattering cross section for the trajectories grazing the nucleus, while the neutron transfer reaction differential cross section for these same trajectories is several orders-of-magnitude less.[3,6–9] Thus, the identification problem for the detection of the N^{13} nuclei is severe. In particular, detection by the usual techniques of scintillation counters, gas counters, or photographic plates is most difficult. Consequently, the detection has been accomplished by exploiting the radioactive property of the N^{13} nuclei, since these nuclei emit 1.2-Mev positrons with a convenient 10-minute half-life. Indeed, this technique has been the common one used heretofore in the study of the N^{14} transfer reactions.[3,6–9]

A drawing of the apparatus used is shown in Fig. 1. The reaction chamber consists of two 12-in. diameter hemispheres which may be quickly separated at the equator by means of swinging captive bolts. The N^{14} beam enters at the north pole (the left hemisphere) through a $\frac{1}{4}$-in. diameter collimator (not shown). A $1\frac{1}{4}$-in. diameter tube extends 3 in. into the hemisphere to shield the walls of the sphere from radiation coming from the collimator. The beam is collected in an external Faraday cup beyond the south pole of the right hemisphere. The 2.2 mg/cm^2 thick gold target is placed at the center of the assembled sphere being mounted on two $\frac{1}{8}$-in, diameter rods based near the north pole. The target is placed with its normal pointing forward, 45° above the beam axis. Longitude lines every 15° and latitude lines every 5° are engraved on the inner face of the hemispheres. The latitude lines denote the angle with respect to the polar beam axis, θ. Detection of the N^{13} nuclei leaving the target is accomplished by collecting the nuclei on $\frac{1}{2}$-in. wide "Scotch" tapes[11] which are positioned along the latitude lines. The $\frac{1}{2}$-in. wide tapes subtend latitude angles of a little less than 5°. The tapes are indicated in Fig. 1 (they cover the longitude lines); they are seen to extend only part way around the sphere. The length of each tape is determined by

[11] Tape No. 472 manufactured by Minnesota Mining and Manufacturing Company, Minneapolis, Minnesota.

the requirement that no detected nucleus should pass through the target at an angle greater than 60° from the normal of the target. From the taped area in Fig. 1 it is seen that something like one half of all the nuclei ejected at a particular angle, θ, are collected by the tapes. Angles between 20° and 160° are available for N^{13} detection. After a 15–20 minute bombardment of the target, the tapes are removed and their radioactivity measured by 10 scintillation counters. A total of 10 tapes can, in this manner, be exposed at one time.

B. Particle Detection Equipment

The 1.2-Mev positron radioactivity of the N^{13} nuclei collected on the tapes is detected by scintillation detectors via the annihilation radiation from the positrons. Each tape is wrapped on an aluminum spool which is then placed inside a $\frac{1}{8}$-in. wall aluminum cylinder. All of the positrons therefore are stopped either in the tape or in the aluminum container. This material then acts as a source of annihilation radiation which is detected by a $1\frac{1}{2}$-in. diameter by 1-in. thick NaI(Tl) scintillator placed on an RCA 6342 photomultiplier. The pulse-height spectrum obtained from the photomulitplier is amplified and the "photopeak" isolated for counting by a Technical Measurements Corporation PA3B Pulse-Height Selector. This selector has independent upper and lower discriminators so that any spread in pulse height may be selected.[12] The background counting rate in the scintillation counter is greatly reduced by this technique of counting only pulses in the relatively narrow "photopeak" region. With 6 in. of lead shielding around each counter a background counting rate of 4 counts per minute is obtained.

Several advantages are inherent in this method for detecting positrons. In addition to the low background mentioned, an important advantage is the small absorption ($\sim$10%) of the radioactivity by the tape itself. Since the tapes have varying lengths and are relatively thick ($\sim$20 mg/cm^2), it would be difficult to detect the positrons directly and still maintain reproducibility among the tapes of varying lengths. Also the tapes are distorted when mounted on the sphere so that their thicknesses are not uniform. A final advantage obtained by detecting the annihilation radiation is the gain of a factor of two in detection efficiency since two gamma rays accompany every positron decay.

The efficiency of the detection equipment was determined by two methods: (1) With a calibrated Na^{22} positron source[13] and (2) By calculating the efficiency using Monte Carlo data for NaI(Tl) efficiency.[14] Care was taken in the calculation to allow for the finite size of the spool and container which hold the radioactive tapes. The efficiency values obtained by the two methods disagreed with each other by 8%. The efficiency value was found to be (3.9 ± 0.2)%.

C. Beam Monitors

The beam monitor used for taking all of the $Au^{197}(N^{14},N^{13})Au^{198}$ reaction data is a Faraday cup mounted at the exit port of the spherical reaction chamber. A clearing magnet is placed several inches in front of the cup to sweep any electrons out of the N^{14} beam being monitored. A second magnet introduces a magnetic field inside the Faraday cup to trap any electrons produced in the cup by the beam. The charge collected by the Faraday cup is stored on a capacitor, the voltage across the capacitor then being a measure of the N^{14} beam collected in the cup. This voltage is measured with an electrometer.[15] When the Faraday cup is used for monitoring the $Au^{197}(N^{14},N^{13})Au^{198}$ reaction a resistance is connected across the charge-storing capacitor so that the charge on the capacitor leaks off with the same 10-minute half-life as that of the N^{13} nuclei which are decaying on the tapes in the sphere. Use of this technique compensates exactly for variations in the N^{14} beam intensity during the 20-minute bombardment of the target. Finally, it is assumed that, over the range of energies used in studying the $Au^{197}(N^{14},N^{13})Au^{198}$ reaction, the charge of each N^{14} ion is seven units. Northcliffe[16] has shown from range-energy measurements that this assumption is valid to an accuracy of a few percent.

A secondary, transmission-type, beam monitor consisting of three parallel 1 mg/cm^2 thick nickel foils is also available and was used for testing purposes. It is placed at the entrance of the sphere. The outer two foils of the monitor are raised to +1000 volts potential so as to collect electrons emitted by the center foil due to the passage of the N^{14} beam through the foils. The dc current of the center foil is then measured to give a quantity proportional to the beam intensity.

The secondary monitor was used in two tests in conjunction with the Faraday cup to check the apparatus. One test checked the efficiency of the magnets used with the Faraday cup. In this test, the magnetic fields before and at the Faraday cup were increased until the ratio between the Faraday cup reading and the secondary monitor reading were constant. Permanent magnets giving higher fields were then used on the Faraday cup for subsequent experiments.

The second use for the secondary monitor was to make range-energy measurements on the N^{14} beam. Aluminum foils were placed inside the sphere between the secondary monitor and the Faraday cup. The ratio of the Faraday cup charge to secondary monitor charge

[12] We are indebted to the Technical Measurements Corporation, North Haven, Connecticut, for developing for us this type of discriminator.

[13] Obtained from the National Bureau of Standards and calibrated to an accuracy of ±2%.

[14] *Beta- and Gamma-Ray Spectroscopy*, edited by K. Siegbahn (Interscience Publishers, New York, 1953), p. 154.

[15] Cary Electrometer, Model 31, Applied Physics Corporation, Pasadena, California.

[16] L. C. Northcliffe, Phys. Rev. (to be published).

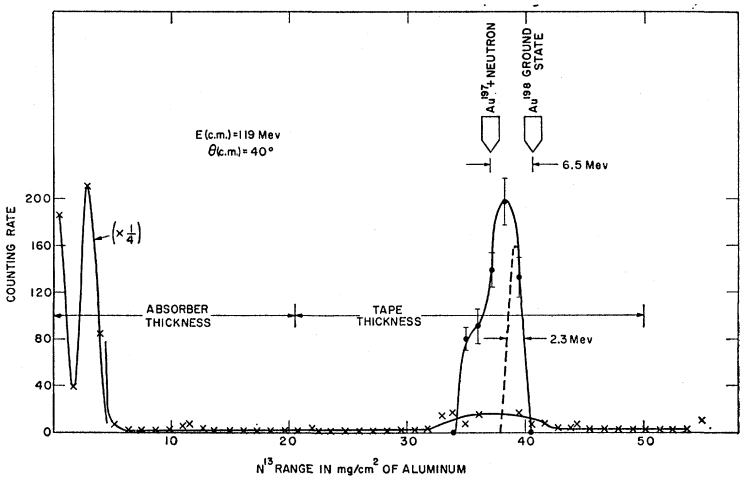

FIG. 2. Range measurement of radioactive products leaving the target at E(c.m.)=119 Mev and θ(c.m.)=40°. The ● points indicate nuclei with a 10-minute half-life (N^{13}). The × points indicate other activities. The broad vertical arrows indicate the N^{13} range expected (1) for neutron transfers to the ground state of Au^{198} and (2) for neutron transfers to the zero energy continuum state of Au^{198}. The width of the arrows reflects the uncertainty in the absolute value of the beam energy. The 2.3-Mev dotted peak indicated under the N^{13} peak represents the maximum energy spread in the N^{14} beam and hence the resolution of the N^{13} range measurement. For normal data-taking conditions, an aluminum absorber stops nuclei leaving the target with ranges less than 20 mg/cm² of aluminum (see left horizontal arrow), while a collecting tape of sufficient thickness captures the N^{13} nuclei (see right horizontal arrow).

was measured as a function of aluminum foil thickness. The range of the N^{14} ions was determined to be the foil thickness at which this ratio dropped to zero.

III. EXPERIMENTAL PROCEDURE

A. Measurement of Beam Energy

A well-collimated N^{14} beam with small energy spread is necessary for the experiment. Thus, the N^{14} beam from the accelerator is deflected, energy analyzed, and deflected again into the reaction chamber after passing through the secondary monitor where a small energy loss occurs. A small energy loss (~1 Mev) also occurs in the gold target.

The energy of the beam was determined by making range-energy measurements (see Sec. II.C). Both a He^4 and a N^{14} beam were passed through the beam deflection system and their ranges measured. The energies of the beams were obtained from the ranges by using the range-energy data of Northcliffe.[16] The magnetic field of the deflection magnet was also determined for each beam by means of a proton moment magnetic field measuring instrument.[17] It was found that the energies obtained from the range measurements were consistent with the magnetic field measurements to within ~1%. The N^{14} beam energy was in this manner determined to be 145.6±1 Mev.

Lower energy N^{14} beams were obtained by using aluminum absorbers to degrade the beam energy to the desired values, the aluminum absorbers being placed at the entrance to the reaction sphere. The energy values were obtained by weighing the absorbers and using Northcliffe's range-energy data.[16]

[17] NMR Precision Gaussmeter, Model G-501, Harvey-Wells Inc., Southbridge, Massachusetts.

B. N^{13} Particle Identification

Four tests were made to insure that the radioactive nuclei being detected were indeed N^{13} which had been produced in the target.

(1) *Half-Life Measurement of* N^{13} *Decay*

When counting the gamma rays from the radioactive tapes, the number of counts detected were recorded each minute. A plot of the counting rate verses time was then made and only the 10-minute decay component was assigned to the N^{13} activity. This measurement was made for all N^{13} data taken and was the primary means of identification.

(2) *Pulse-Height Analysis of* N^{13} *Decay Products*

Spot checks were made to determine that the pulse-height distribution obtained from the scintillation counters gave a typical annihilation radiation distribution.

(3) *Range Measurement of* N^{13} *Nuclei*

By placing a stack of thin (1.12 mg/cm²) aluminum strips at one angle the ranges of the various nuclei at that angle were determined. The results obtained for a center-of-mass beam energy of 119 Mev are displayed in Fig. 2, where the relative number of counts per foil is plotted against the depth of the foil in the stack. The points denoted with the ● indicate that a 10-minute half-life was obtained at that point. The 10-minute half-life points are all clustered in the region of 40 mg/cm². The broad vertical arrows above the points indicate the range of N^{13} expected for (a) the transfer of a neutron from N^{14} to the ground state of Au^{198}, and (b) the stripping of a neutron from N^{14} such that the neutron is unbound and has zero energy. The ranges of the N^{13} nuclei fall into the region between the arrows. In addition to the desired long-range N^{13} nuclei, Fig. 2 shows

that there are also a great many short-range nuclei. The shortest range nuclei are presumably spallation products from the target; the nuclei of range 3 mg/cm^2 are most likely fission fragments. These nuclei were all eliminated when studying the N^{13} angular distributions by using a 20.5 mg/cm^2 thick aluminum shell inside the reaction chamber between the target and the tapes on the wall. This shell absorbed the short-range nuclei as indicated by the horizontal arrows in Fig. 2. The thickness of the collecting tape is also indicated by an arrow in Fig. 2. All runs were taken with sufficient aluminum absorber to insure that the N^{13} nuclei were stopped in the tape. From Fig. 2 it is clear that almost all of the nuclei collected on the tape are the desired N^{13} nuclei.

(4) *Test for Spurious* N^{13} *Activity*

It is possible for N^{13} nuclei that have not originated in the target to be collected in the tapes: (a) N^{14} nuclei scattered out of the beam by the target may convert to N^{13} nuclei upon striking the tapes, or (b) N^{13} nuclei in the accelerator beam may be elastically scattered by the target and be collected in the tapes. The angular distribution for each case should decrease with angle approximately according to the Rutherford scattering law. Since the desired (N^{14},N^{13}) reaction in the target produces N^{13} nuclei only in the neighborhood of one angle, the smoothly falling spurious angular distribution should be easy to subtract. Nevertheless, a test was made to determine the contribution to the N^{13} activity in the tapes due to these mechanisms.

The accelerator beam was used to bombard directly tapes of the type used for collecting the N^{13} nuclei. These tapes were placed in the Faraday cup during bombardment. The resulting N^{13} activity measured in these tapes was then known to be produced by the two mechanisms considered above (but without the intervening scattering process): (a) N^{14} to N^{13} conversion in the tapes, and (b) collection of N^{13} already in the beam. From this measured activity and the additional consideration of the Rutherford scattering cross section, the N^{13} activity in the tapes in their usual positions, due to these two mechanisms, was calculated. The activity was found to be negligible in comparison to the activity produced by the desired (N^{14},N^{13}) reaction in the target.

C. Determination of the Energy Resolution

The energy resolution of the N^{14} beam was measured by doing an elastic scattering measurement and noting the energy resolution of the scattered N^{14} nuclei. These nuclei were detected with a CsI(Tl) scintillator. The energy spectrum of the N^{14} nuclei was found by this method to have a width of 2.3 Mev at a bombarding energy of 119 Mev (same conditions as in Fig. 2). This energy spread value is an *upper limit* since the contribution to the spread from the CsI(Tl) detector is included in the value.

The 2.3-Mev value for the energy spread is plotted under the N^{13} peak in Fig. 2. (The contribution to the energy spread due to straggling in the aluminum absorber foils is negligible.) It is clear from Fig. 2 that the instrumental energy spread of the N^{14} nuclei in the beam is much smaller than the energy spread of the N^{13} nuclei leaving the Au^{197} target. Therefore, the energy spread of the N^{13} nuclei must be a result of the interaction of the N^{14} nuclei with the Au^{197} nuclei. Either the resulting Au^{198} nuclei are left in discrete excited states or, if more than 6.5 Mev of energy is lost by the N^{13} nuclei, the neutron has been transferred to Au^{198} continuum states.

Two of these possibilities are exhibited in Fig. 2 by means of the two broad vertical arrows which indicate the range expected for N^{13} nuclei when either the Au^{198} nuclei are left in the the ground state or the transferred neutron remains free. The widths of the arrows are introduced because of the uncertainty in the energy of the beam of N^{14} nuclei. These widths do not affect the energy resolution; they merely reflect the uncertainty in the relation between the abscissa in Fig. 2 (the range) and the absolute energy. From inspection of Fig. 2 it may be concluded, therefore, that the neutron from the N^{14} nucleus is being transferred to nuclear states other than the ground state of Au^{198} and quite likely to states in the Au^{198} continuum.

There is also an energy effect introduced by the thickness of the target: $N^{14} \rightarrow N^{13}$ transfers taking place as the beam enters the target occur at higher energies than those transfers taking place as the beam leaves the target. This effect does *not* affect the energy spread of the N^{13} nuclei leaving the target but it does introduce a

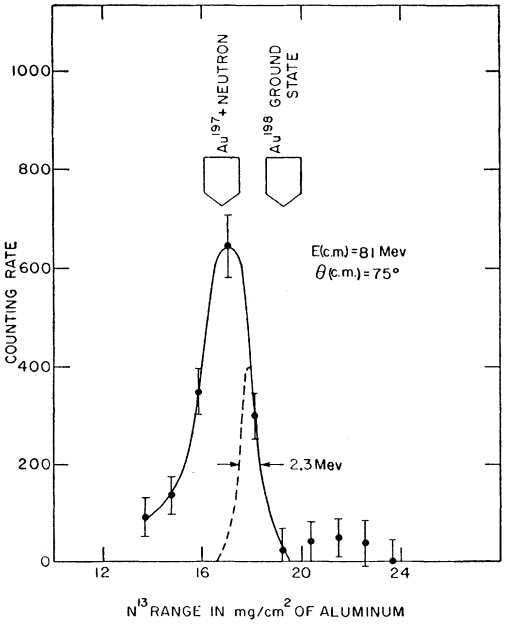

FIG. 3. Same as Fig. 2 except E(c.m.)=81 Mev and θ(c.m.)=75°.

spread in the energy at which the transfer process takes place. This effect introduces a spread of at most ± 2 Mev in the center-of-mass energy for the transfer process.

As a check on all of the range measurements a second absorption curve was taken for the N^{13} nuclei when the N^{14} beam energy was considerably lower than in Fig. 2, namely, E(c.m.)$=81$ Mev. The results obtained are shown in Fig. 3 and are seen to be similar to those shown in Fig. 2.

D. Angular Distribution Measurement

The basic measurement made in the experiments reported here is that of the angular distribution of the N^{13} nuclei. This measurement was performed at 15 different energies. A number of measurements were repeated so that, in all, 25 different angular distributions were taken.

The procedure was to expose ten tapes at ten different angles. In this manner the entire angular distribution was obtained at once. Thus, the relative values of the cross sections obtained at different angles are limited in their accuracy only by the statistics of the counting. An estimate of the accuracy of the data may be obtained by inspection of Figs. 4 and 5. Figure 4 shows the angular distribution obtained at the highest energy studied [E(lab)$=142$ Mev], Fig. 5, the distribution for the lowest energy studied [E(lab)$=74$ Mev]. Angular distributions were actually taken at two lower energies so that total cross sections could be obtained, but the statistics at these energies restricted the use of data to the total cross-section work. Inspection of Figs. 4 and 5 shows that at the highest

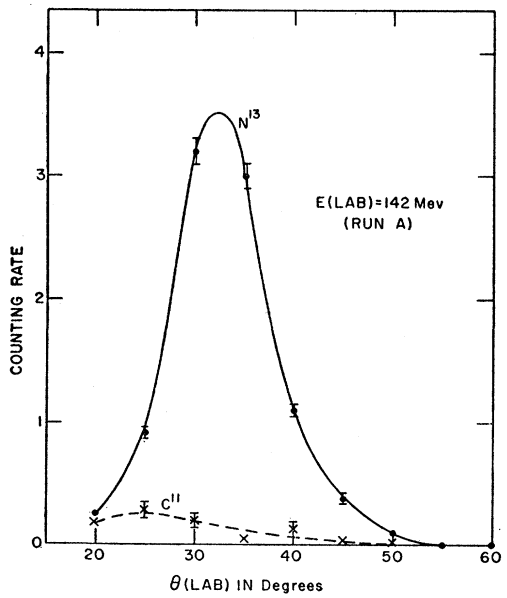

FIG. 4. An angular distribution measurement taken at E(lab) $=142$ Mev. The ● points are for N^{13} nuclei, the × points are for C^{11} nuclei.

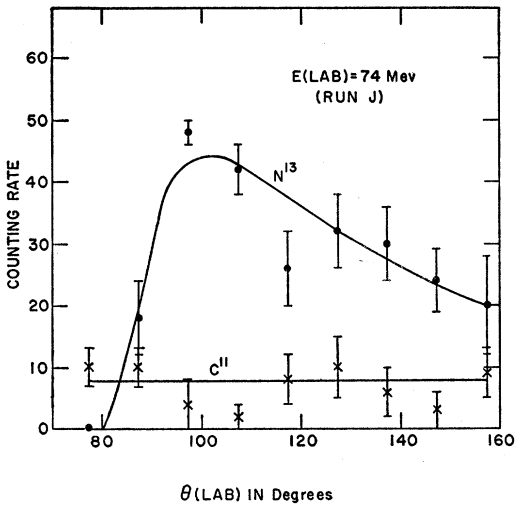

FIG. 5. Same as Fig. 4 except for E(lab)$=74$ Mev.

energy the C^{11} background is negligible while even at the lowest energy the N^{13} curve is definitely defined.

The deviations in the values for the points shown in Figs. 4 and 5 are somewhat subjective. The raw data consist of experimental decay curves which are fitted by eye to a master curve composed of 10-minute (N^{13}) and 20-minute (C^{11}) half-lives. The deviations indicate something like 80% certainty of the experimental value lying inside the error bars.

The angular resolution of the experiment is determined by the spread in angle covered by the collecting tapes and by the geometrical size of the N^{14} beam striking the target since the multiple scattering by the target and the energy degrading foils is negligible compared to these factors. Either one $\frac{1}{2}$-in. tape ($\sim 5°$ angular spread) or two $\frac{1}{2}$-in. tapes ($\sim 10°$ angular spread) were used at each scattering angle investigated, depending on the counting rate obtained. The $\frac{1}{4}$-in. beam spot on the target thus added little to the spread in scattering angles detected.

Total cross sections are obtained by summing over the measured differential cross sections.

IV. RESULTS AND DISCUSSION

A. Differential Cross Sections

The experimental differential cross sections $d\sigma/d\Omega$ for the production of N^{13} in the ($Au^{197}+N^{14}$) reaction in the center-of-mass system are presented in Fig. 6. Letters indicate experimental values, a letter being assigned to each energy. The lower portion of Fig. 6 plots ten times $d\sigma/d\Omega$ to reveal more details. A qualitative discussion of the behavior of the experimental peaks has been given already in the Introduction and Summary (Sec. I). In this section, the more quantitative aspects will be presented.

As discussed in Sec. I, it is convenient to plot the differential cross sections as functions of $R_{\min}$, the

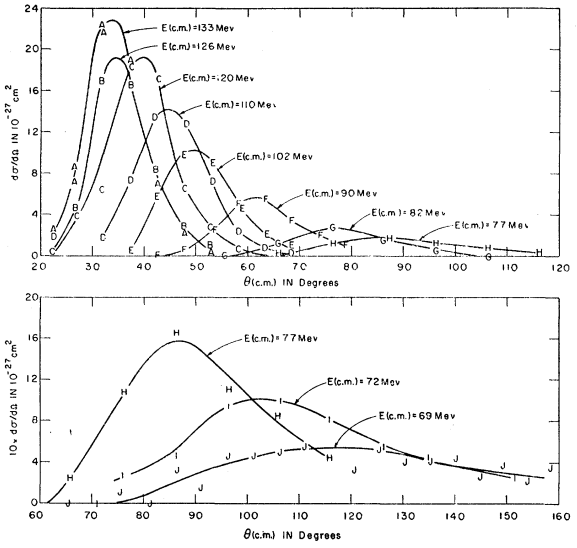

FIG. 6. Summary of angular distribution measurements ($d\sigma/d\Omega$ plotted against θ(c.m.)). The letters are plotted to indicate measured differential cross-section values. A different letter is assigned for each bombarding energy. The curves are smooth lines drawn through the experimental data. The lower portion of the figure shows the cross sections plotted with a magnification of 10 to reveal more details.

distance of closest approach to the gold nucleus of the classical trajectories of the nitrogen nuclei. Using Rutherford scattering trajectories, $R_{\min}$ is related to the center-of-mass deflection angle θ and the center-of-mass energy E by

$$R_{\min}=a'[1+\csc(\theta/2)], \tag{1}$$

where

$$a'=ZZ'e^2/2E. \tag{2}$$

Here, Ze and $Z'e$ are the charges of the N^{14} and Au^{197} nuclei. The desired differential cross section, $d\sigma/dR_{\min}$, may be determined from the $d\sigma/d\Omega$ value by means of Eq. (1) since

$$\frac{d\sigma}{dR_{\min}}=\frac{d\sigma}{d\Omega}\frac{d\Omega}{d\theta}\frac{d\theta}{dR_{\min}},$$

$$d\Omega/d\theta=2\pi\sin\theta,$$

and

$$dR_{\min}/d\theta=-(a'/2)\cos(\theta/2)\csc^2(\theta/2), \tag{3}$$

$$d\sigma/dR_{\min}=-(8\pi/a')\sin^3(\theta/2)d\sigma/d\Omega. \tag{4}$$

The $d\sigma/dR_{\min}$ values corresponding to the $d\sigma/d\Omega$ cross sections plotted in Fig. 6 have been calculated by means of Eq. (4) and have been plotted on a logarithmic scale in Fig. 7. All data for each energy in Fig. 7 have been arbitrarily normalized to unity at their maximum values. The letters still indicate experimental quantities. Although the peaks coincide nicely for all of the data, there is a noticeable widening of the peaks on the large $R_{\min}$ side of the peak when the energy is increased (for the earlier letters in the alphabet.) Part of this effect can be accounted for as follows. Experimentally, $d\theta$ is a constant and so, at the smaller angles, $dR_{\min}$ becomes quite large because of the $\csc^2(\theta/2)$ dependence of $dR_{\min}/d\theta$ in Eq. (3). Thus, at 20° and at the highest energy (A points), the $d\theta$ value of 5° transforms to a $dR_{\min}$ magnitude of 3.5×10^{-13} cm. Such spreads in $dR_{\min}$ have been indicated in Fig. 7 by horizontal bars. Even when this effect is included, however, the higher energy peaks in Fig. 7 remain somewhat wider than the low-energy peaks.

The distorting effect of the $dR_{\min}/d\theta$ transformation can also be used to explain the large interaction radius reported by Hubbard and Merkel.[8] Their peak in $d\sigma/d\Omega$ was obtained at $\theta=18°$. Use of Eq. (1) by them yielded a value of $r_0=1.96\times10^{-13}$ cm where r_0 is defined by $R_{\min}=r_0(A_1^{\frac{1}{3}}+A_2^{\frac{1}{3}})$, A_1 and A_2 being the atomic weights of the two nuclei in the interaction. If, however, $d\sigma/dR_{\min}$ is calculated from $d\sigma/d\Omega$ by means of Eq. (4), the peak value of $d\sigma/dR_{\min}$ is found to correspond to the $\theta=25°$ datum. This occurs because of the $\sin^3(\theta/2)$ term in Eq. (4) which depresses the small-angle data. If $\theta=25°$ is used as the angle for the grazing trajectory, then r_0 is found to be 1.54×10^{-13} cm is good agreement with the present data.

Comparison will now be made between the experimental data and the tunneling theory of Breit and Ebel.[4] They give, in Eq. (23.1) of reference 4, the following angular-dependent terms for the tunneling differential cross section, $d\sigma/d\Omega$:

$$\csc^3(\theta/2)\exp[-2\alpha a'\csc(\theta/2)]. \tag{5}$$

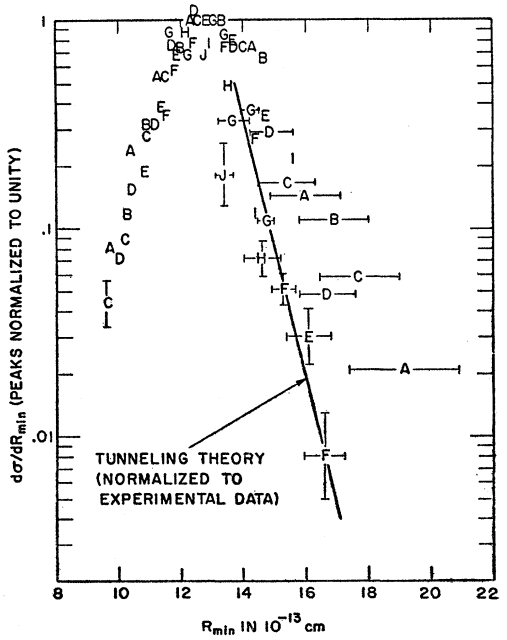

FIG. 7. The differential cross sections, $d\sigma/dR_{\min}$, plotted against $R_{\min}$ on a logarithmic scale. The letters indicate experimental values which are obtained from the experimental values plotted in Fig. 6 by means of the transformation given in Eq. (4). The data for each energy are normalized to unity at the maximum value for $d\sigma/dR_{\min}$ at that energy. The curve is calculated from the tunneling theory of Breit and Ebel[4] as given in Eq. (6) and is normalized to fit the experimental points.

Here, α is the decay constant for the wave function of the neutron bound in the N^{13} nucleus; its value[18] is 0.715×10^{13} cm^{-1}. If, now, $d\sigma/d\Omega$ is transformed to $d\sigma/dR_{\min}$ by means of Eq. (4) and the energy dependent terms dropped, using Eq. (1), the angular dependence of $d\sigma/dR_{\min}$ is found to be proportional to

$$\exp(-2\alpha R_{\min}). \quad (6)$$

Equation (6) shows that, aside from a normalizing coefficient which contains energy factors, $d\sigma/dR_{\min}$ is a function only of $R_{\min}$. Thus, if consideration is limited to the dependence of $d\sigma/dR_{\min}$ on the exponential factor in Eq. (6), and other energy dependent factors are neglected, a comparison between the experimental data and the tunneling theory may be made by normalizing the experimental data obtained at different energies to give the same peak value for $d\sigma/dR_{\min}$. A universal curve has been drawn in Fig. 7, using Eq. (6), for comparison with such normalized experimental data. The only parameter in Eq. (6) is α, which is determined by the binding energy of the transferred neutron.

The curve derived from the tunneling theory as given in Eq. (6) is plotted in Fig. 7; it is normalized to fit the lower energy data. The tunneling curve would be expected, of course, to fit only the data at the large values of $R_{\min}$, i.e., for trajectories which do not penetrate the absorption radius R_a. It is seen that the data (for example, the F points) are represented quite well by the tunneling curve. It may be concluded therefore that, for some bombarding energies at least, the angular dependence of the differential cross sections is in agreement with the tunneling mechanism.

B. Total Cross Sections

The total cross section, σ, for the neutron transfer process is obtained for each energy by summing over the differential cross sections for that energy. The resulting experimental values are plotted against the center-of-mass energy, E(c.m.), in Fig. 8. It is seen that the cross section points rise rapidly with energy until a value of about 10^{-26} cm^2 is reached at which point there is a leveling off of the data. The sharp rise occurs as the bombarding energy is increased because the N^{14} trajectories penetrate more closely to the Au^{197} nucleus at the higher energies; the strong dependence of the transfer cross section on nuclear radius (see Fig. 7) therefore enhances the high-energy cross sections. However, as the bombarding energy is further increased the N^{14} trajectories begin to pass inside the absorption radius, R_a. Nuclei on these trajectories are absorbed and so do not contribute to the transfer cross section and the cross-section values level off.

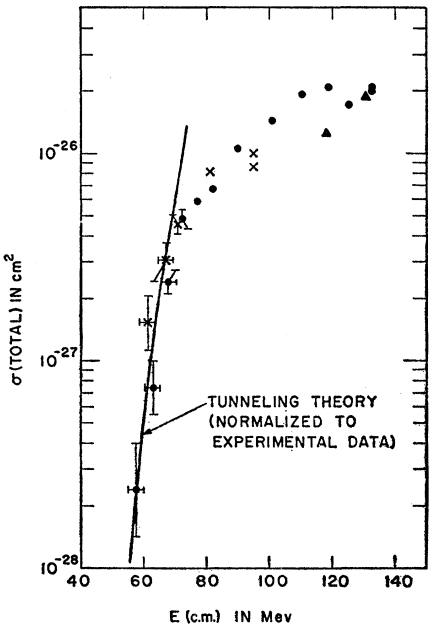

FIG. 8. Total cross sections plotted against beam energy. The ● and × points indicate results obtained on two different days. The curve is obtained from the tunneling theory of Breit and Ebel[4] as given in Eq. (7).

It is clear, therefore, that only the steeply rising part of the total cross-section data is associated solely with the transfer mechanism while the level portion includes also the effect of nuclear absorption. A comparison can be made then between the tunneling theory of Breit and Ebel[4] and the steep portion of the data in Fig. 8. Using the expression for the total cross section as given in Eq. (25.2) of reference 4, a ratio for the total tunneling cross section, $\sigma(E)$, at two different energies, E_1 and E_2, was obtained:

$$\sigma(E_1)/\sigma(E_2) = (E_2/E_1)\exp[-2\alpha ZZ'e^2(E_1^{-1}-E_2^{-1})]. \quad (7)$$

Normalizing $\sigma(E_2)$ to the data in Fig. 8, $\sigma(E_1)$ was calculated for a number of energies and is shown plotted as a curve in that figure. It is seen that the tunneling curve fits the experimental data well.

V. ACKNOWLEDGMENTS

We wish to thank Professor G. Breit for suggesting that we study the nucleon transfer reaction. We are also indebted to him for many very helpful discussions about this work. The reaction chamber was designed and built for us by A. Nicolaeff, A. Disco, and A. Massini. S. D. Baker and K. H. Wang have assisted in the collection and analysis of the data. Finally, we are indebted to the accelerator crew under the direction of Dr. M. S. Malkin for the reliable operation of the heavy-ion accelerator.

[18] This value assigned to α is strictly correct only for a reaction with a Q of zero. The value used corresponds to a binding energy of 10.55 Mev for the neutron in the N^{13} nucleus. Breit, reference 2, Eq. (48.79′), has given an approximate expression for α when the Q value is not zero. For the $Au^{197}(N^{14},N^{13})Au^{198}$ reaction, the Q value is -4.06 Mev if the neutron is captured in the ground state of the Au^{198} nucleus. For capture in the other states (which captures are also measured experimentally), the Q would be even more negative. Thus, it is not clear just what value of α should be used. The value used is therefore to be considered only as a first approximate representation of the situation.